

# LOW-LEVEL ATMOSPHERIC JETS AND INVERSIONS OVER THE WESTERN WEDDELL SEA \*

EDGAR L. ANDREAS<sup>1</sup>, KERRY J. CLAFFEY<sup>1</sup> and ALEKSANDR P. MAKSHITAS<sup>2</sup>

<sup>1</sup>*U.S. Army Cold Regions Research and Engineering Laboratory, 72 Lyme Road, Hanover, New Hampshire 03755-1290, U.S.A.*; <sup>2</sup>*International Arctic Research Center, 930 Koyukuk Drive, Fairbanks, Alaska 99775-7335, U.S.A.*

(Received in final form 26 April 2000)

**Abstract.** For four months in the fall and early winter of 1992, as Ice Station Weddell (ISW) drifted northward through the ice-covered western Weddell Sea, ice station personnel profiled the atmospheric boundary layer (ABL) with radiosondes. These showed that the ABL was virtually always stably stratified during this season: 96% of the soundings found a near-surface inversion layer. Forty-four percent of these inversions were surface-based. Eighty percent of the soundings that yielded unambiguous wind profiles showed an atmospheric jet with speeds as high as  $14 \text{ m s}^{-1}$  in a core below an altitude of 425 m. This paper documents the features of these inversions and low-level jets. Because the inversion statistics, in particular, are like those reported in and around the Arctic Ocean, similar local processes seem to control the ABL over sea ice regions in both hemispheres. A simple two-layer model, in which an elevated layer becomes frictionally decoupled from the surface, does well in explaining the ISW jet statistics. This model also implies a new geostrophic drag parameterization for sea-ice regions that depends on the magnitude of the geostrophic wind, the 10-m drag coefficient  $C_{DN10}$ , and the ABL height, but not explicitly on any stratification parameter.

**Keywords:** Geostrophic drag relation, Inertial oscillations, Inversions, Low-level jet, Stable boundary layer, Weddell Sea.

## 1. Introduction

The theme that the polar regions are ideal ‘laboratories’ for studying atmospheric processes is a recurring one in the meteorological literature (e.g., Lettau, 1971; Smith et al., 1983; Andreas and Cash, 1999). We reiterate that theme here and demonstrate it with a study of the stable atmospheric boundary layer (ABL) at Ice Station Weddell (ISW).

Our understanding of the stable boundary layer (SBL) lags that of the convective boundary layer (CBL) because, in temperate latitudes, the SBL is generally only a nighttime phenomenon. Since the SBL takes longer to develop than the CBL (Nieuwstadt and Duynkerke, 1996), it frequently does not reach steady state by sunrise in mid-latitudes; its characteristics are, thus, difficult to quantify. In the polar regions, on the other hand, the low sun angle, the highly reflective and emissive

\* The U.S. government right to retain a non-exclusive royalty-free license in and to any copyright is acknowledged.



snow surface, and the long polar nights combine to produce frequent and long-lasting SBLs. During our 4-month deployment on ISW, for example, virtually all of our radiosoundings showed a stably stratified ABL. In other words, we found nearly ideal conditions for an SBL experiment.

Here we report on two features of the SBL over sea-ice that our radiosounding program on Ice Station Weddell revealed: low-level atmospheric jets and inversions. Over 96% of our 164 radiosoundings on ISW showed a low-level temperature inversion with its top below 600 m. And 80% of the soundings for which we measured the wind vector as well as temperature showed an atmospheric jet with its core below 425 m. Andreas et al. (1993, 1995), Claffey et al. (1994), and Makshtas et al. (1998) made preliminary reports on these jets and inversions. Here we document details of both the inversions and jets and describe a simple model of inertial oscillations in a layer decoupled from the surface by stable stratification that explains the jet observations. This model also implies a new formulation for the geostrophic drag relation over sea-ice.

## 2. Measurements

Ice Station Weddell drifted through the western Weddell Sea for four months in the austral fall and winter of 1992 (Figure 1), basically following the course of the legendary *Endurance* (Anonymous, 1992; ISW Group, 1993). The Russian icebreaker *Akademik Fedorov* deployed the ice camp in early February near 51° W, 71° S; the *Fedorov* and the U.S. icebreaker *Nathaniel B. Palmer* retrieved the camp in early June near 53° W, 66° S.

On ISW we launched radiosondes twice a day, at 0000 UT and 1200 UT, to investigate the structure of the ABL. Claffey et al. (1994) reported the details of our radiosounding program. That report includes a list of all the ISW soundings and also the soundings made on the *Fedorov* in late May and early June as it approached the camp from the northeast, tabulates some of the statistics we report here, and plots all the ISW and *Fedorov* soundings. In addition, electronic files of these soundings are available from us and from the CRREL library.

We used two types of radiosondes on ISW: tether sondes and air sondes (both made by Atmospheric Instrumentation Research, Boulder, Colorado). The tether sonde was our preferred sounding system because, besides pressure, temperature, and humidity, it also measured wind speed with a cup anemometer and wind direction using the aerodynamically shaped balloon as a vane. But for surface winds above 5–7 m s<sup>-1</sup>, it was hazardous to launch the tether sonde. In these cases, we made the scheduled sounding with a disposable airsonde, which measured only pressure, temperature, and humidity.

The tether sonde was tethered to a winch. We raised the balloon and sonde at a rate of 1–2 m s<sup>-1</sup>. The tether sonde had a 10-s sampling interval and, thus, gave us excellent vertical resolution of 10–20 m. The air sondes generally ascended at

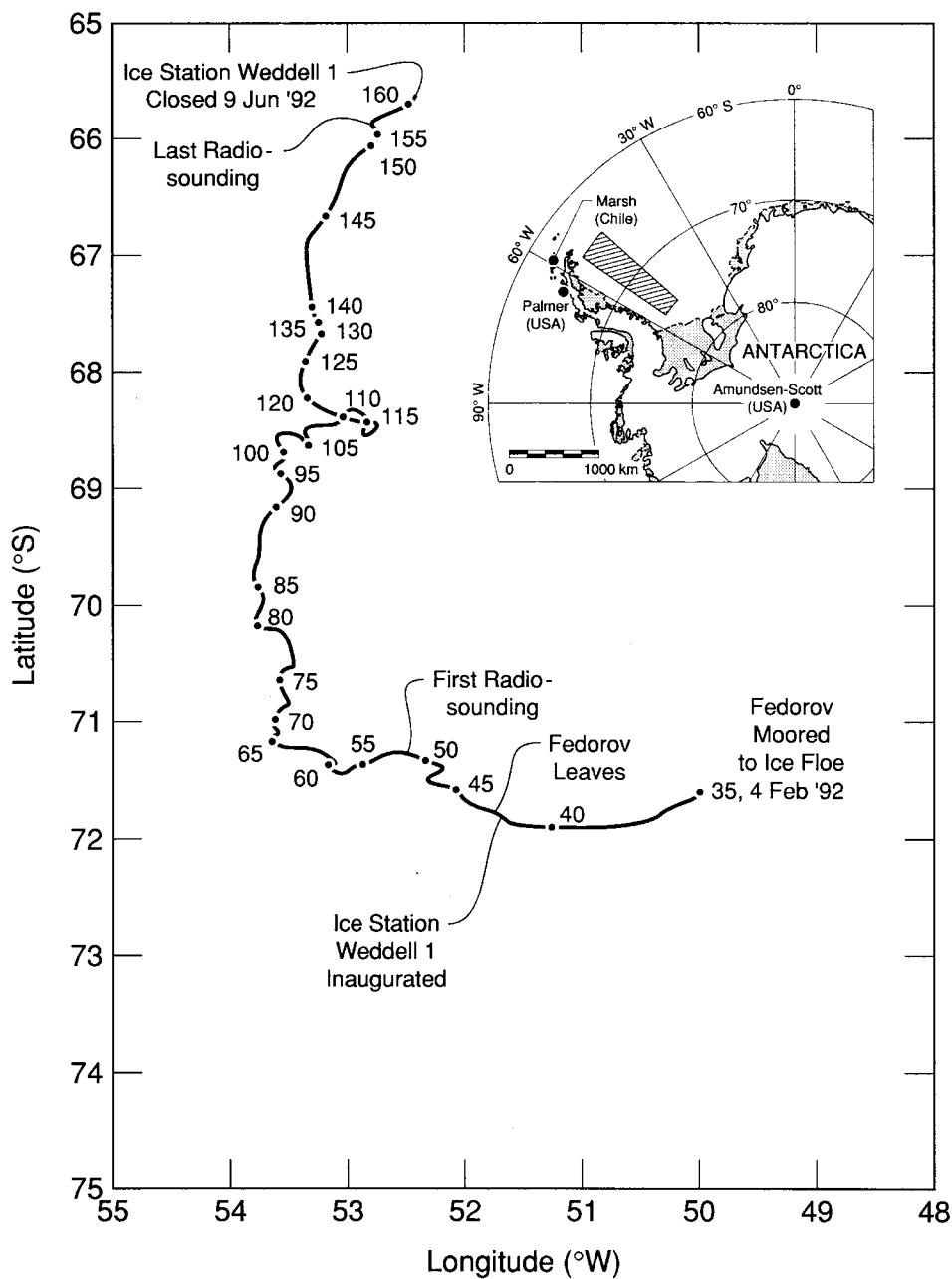


Figure 1. The drift track of Ice Station Weddell, showing station highlights and the duration of our radiosounding program. The numbers indicate the Julian day in 1992.

about  $5 \text{ m s}^{-1}$ . Because this system had a sampling rate of 5 s, it also provided a respectable vertical resolution of 20–25 m.

The *Fedorov* used a Vaisala MicroCORA for 40 6-hourly soundings in late May and early June that were coordinated with soundings at the ice camp. This system measured pressure, temperature, and humidity as well as wind speed and direction using the Omega navigational aid signals (e.g., Andreas and Richter, 1982). The MicroCORA had a 10-s sampling interval, and the balloon typically ascended at  $5 \text{ m s}^{-1}$ ; thus, pressure, temperature, and humidity have a resolution of about 50 m. But the system needed several Omega fixes on the radiosonde to compute wind speed and direction. Consequently, the MicroCORA profiles have a vertical resolution that is generally no better than 100 m for wind data.

Because of this coarser resolution of the MicroCORA data, we could not compare ice camp and *Fedorov* soundings in detail. Claffey et al. (1994) and Makshtas et al. (1998) described our attempts at such comparisons and showed that gross details, such as the frequency of inversions, the temperature of the inversion base, and the temperature difference through the inversion, were comparable at the *Fedorov* and at the ice camp, despite separations up to several hundred kilometres. We infer from these comparisons that the bulk thermal structure of the ABL over the ice-covered Weddell Sea did not have large horizontal variations. But the MicroCORA simply did not have the vertical resolution to provide the details of the jets and inversions that we see in the ice camp soundings. Hence, we will discuss the *Fedorov* soundings no further.

On ISW we made 164 soundings between 21 February and 4 June 1992; 129 were made with the tethersonde and, thus, include profiles of wind speed and direction as well as pressure, temperature, and humidity. Because we tended to launch an airsonde rather than the tethersonde when the surface wind was above  $5\text{--}7 \text{ m s}^{-1}$ , the statistics we report for the low-level jets might be somewhat biased. According to the definition that we will present shortly, jets are more probable when the surface wind is light. Thus, since about 80% (= 129/164) of our soundings were made with the tethersonde, our statistics could be biased by 20%. High winds, however, did not necessitate all of the 35 airsonde ascents (i.e., 164 – 129). The tethersonde experienced some losses and equipment failures that grounded it when wind conditions were otherwise acceptable for launching; Claffey et al. (1994) described these equipment problems.

To further investigate any possible sampling bias, from the standard meteorological observations on ISW (e.g., Andreas and Claffey, 1995), we (Makshtas et al., 1998) created a subset of wind speed observations made at 0000 UT and 1200 UT for the duration of the drift. From this set, we created another subset of the 0000-UT and 1200-UT wind speeds measured only during tethersonde launches. Both wind speed sets followed a Rayleigh distribution with standard deviations of 3.88 and  $3.27 \text{ m s}^{-1}$ , respectively. Using Pearson's  $\chi^2$  test, we found that the two subsets came from the same population with 95% probability or better. Consequently, at

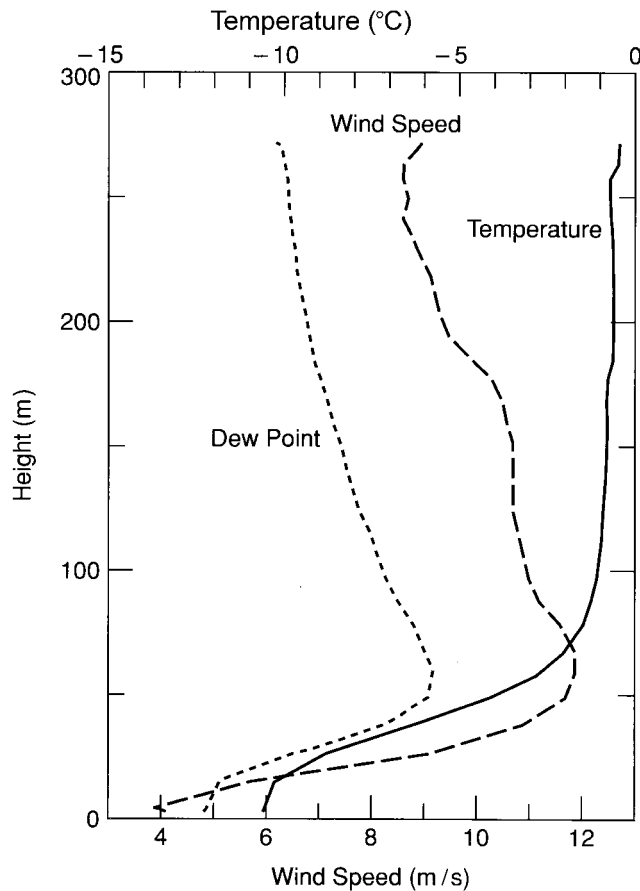


Figure 2. A tethersonde sounding made on Ice Station Weddell at 1200 UT on 19 April 1992. The variables plotted are temperature, dew-point temperature, and wind speed.

least for surface-level wind speeds between 0 and  $7 \text{ m s}^{-1}$ , the tethersonde profiles do not seem to have come from a biased population.

### 3. Results

Figure 2 shows an example of an ISW sounding made with the tethersonde. The fine resolution in the sounding data allows us to identify here a surface-based inversion whose top is at 212 m and a jet in the wind speed profile with a core speed of  $11.9 \text{ m s}^{-1}$  at 68 m above the surface.

Of our 164 ISW soundings, two were too short to show clear evidence of an inversion, four showed no low-level inversion, and 158 (96.3%) showed a temperature inversion layer with its top below 600 m. Of the 103 tethersonde soundings for which we could unambiguously decide whether or not there was a low-level jet,

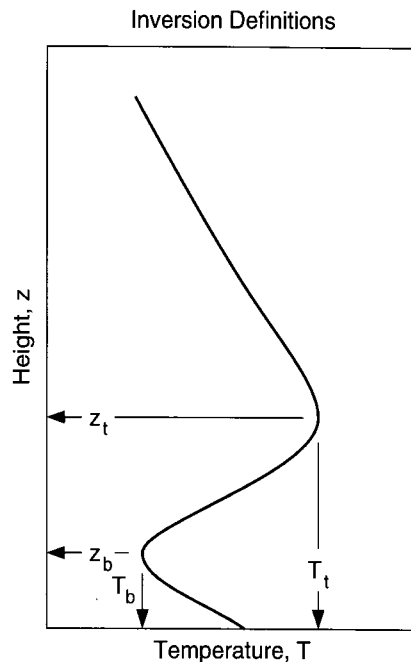


Figure 3. Parameters of a low-level temperature inversion.  $z_b$  is the height of the base of the inversion;  $T_b$  is the temperature there.  $z_t$  is the height at the top of the inversion;  $T_t$  is the temperature there (see Kahl, 1990).

82 (79.6%) showed a jet with a core below 425 m. We elaborate below on these observations.

### 3.1. LOW-LEVEL INVERSIONS

We used Kahl's (1990) protocol to identify an inversion. Figure 3 defines our terminology. To find inversion parameters, we scanned up each temperature profile. If the temperature at a level increased, we called the level immediately below it the base of the inversion and used its values of height and temperature for  $z_b$  and  $T_b$ , the height of the inversion base and the temperature there. As we continued to scan upward, if the temperature at a subsequent level decreased, we called the level immediately below it the top of the inversion and used its values of height and temperature for  $z_t$  and  $T_t$ , the height of the top of the inversion and the temperature at the top. We did, however, ignore thin layers (100 m thick or less) with slightly negative lapse rates that were embedded within a deeper inversion (cf. Kahl, 1990). As we said, this method identified a low-level inversion in over 96% of the soundings.

Figure 4 shows histograms of inversion statistics. Sixty-eight (44%) of the inversions were surface-based, and over 60% had a base below 100 m (Figure 4a). Our incidence of surface-based inversions is roughly what Kahl (1990) and Serreze

et al. (1992) reported for coastal and sea-ice sites in the Arctic Ocean. Since our observations were in autumn and early winter, the temperature at the inversion base was always less than 0 °C (Figure 4b).

Figures 4c and 4d show the depth of the inversion,  $z_t - z_b$ , and the temperature change through the inversion,  $T_t - T_b$ . Although we could identify an inversion and, thus, the inversion base in 158 soundings, many of our soundings did not reach high enough to show the top of the inversion. As a result, Figures 4c and 4d do not contain 158 observations.

Figure 4c shows that the inversions were fairly thin; most were thinner than 550 m. Kahl (1990) and Serreze et al. (1992) reported thicker inversion layers in fall and winter over Arctic sea-ice and at Arctic coastal sites. Because of the finer vertical resolution of our sondes, we put more faith in the ISW inversion statistics. The radiosoundings on which Kahl and Serreze et al. based their analyses had coarser vertical resolution because of sensor response time, balloon ascent rate, and sampling interval, as discussed by Skony et al. (1994), Walden et al. (1996), and Mahesh et al. (1997).

The temperature change through the inversion (Figure 4d) can be quite dramatic, up to 20 °C. Usually, though, that temperature change is more modest, 5 to 10 °C. Figure 4d agrees fairly well with Kahl's (1990) analysis based on autumn and winter observations at Barrow and Barter Island, Alaska. The analysis by Serreze et al. (1992), based on radiosoundings at Russian coastal and island stations, suggests more modest temperature changes through the inversion layer; their median values generally range from 2 to 6 °C. Again, though, these differences in the Russian data used by Serreze et al. could be due to differences in sensor response time and sampling protocol, as explained above.

In summary, our ISW radiosounding program established that low-level temperature inversions are common in autumn and early winter over compact sea-ice in the western Weddell Sea. Despite differences in sounding technology, the ISW inversion statistics do not seem to be markedly different from similar inversion statistics observed at Arctic coastal and sea-ice sites during the same seasons. We thus suggest that the atmospheric boundary layer over Arctic and Antarctic sea-ice regions tends to be locally controlled in the autumn and winter. In other words, the sea-ice surface, the ABL, the clouds, and the sky in both the Arctic and the Antarctic are in quasi-equilibrium because the equilibration time scale is shorter than the time scale of advective events. Makshtas et al. (1999) made the same point, at least about winter, for the two regions.

### 3.2. LOW-LEVEL JETS

Figure 5 defines parameters of the low-level jets. If the wind speed profile shows a local maximum that is 2 m s<sup>-1</sup> higher than speeds both above and below it, we call the feature a jet. Notice, with this definition, the jet must be elevated and cannot occur at the surface. This definition is similar to Stull's (1988, p. 521),

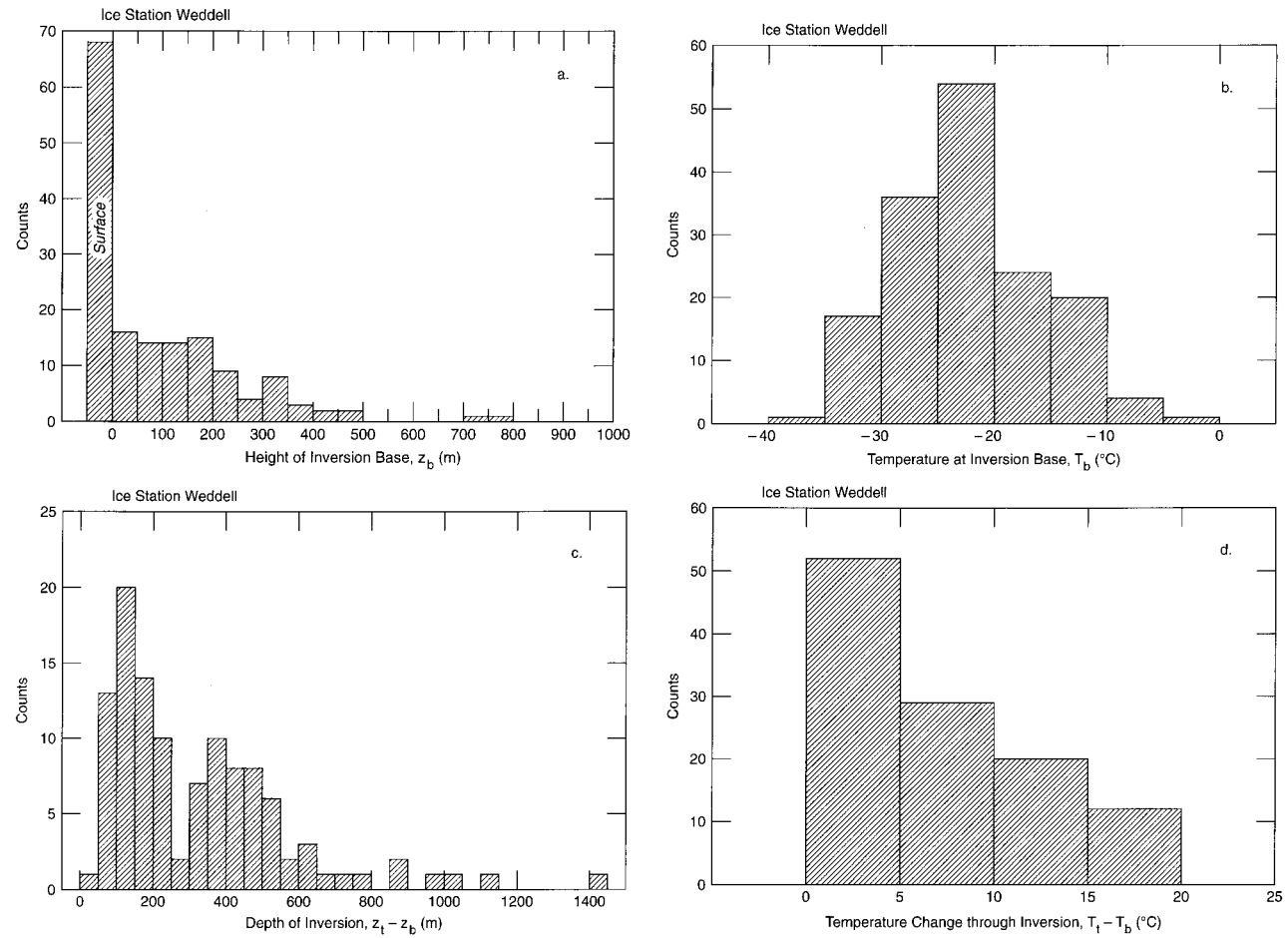


Figure 4. Histograms of inversion statistics as observed on Ice Station Weddell. Panel a shows the height of the inversion base ( $z_b$ ); panel b, the temperature at the inversion base ( $T_b$ ); panel c, the depth of the inversion ( $z_t - z_b$ ); and panel d, the temperature change through the inversion ( $T_t - T_b$ ).

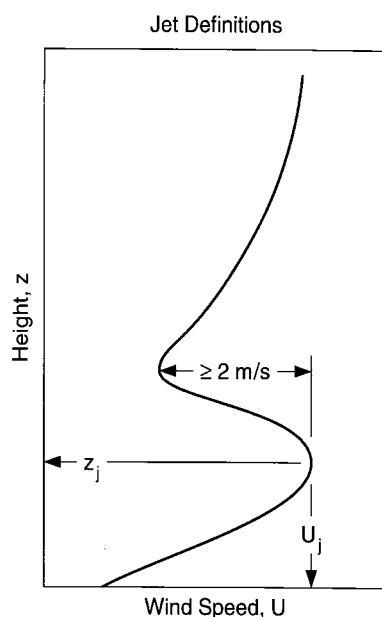


Figure 5. Parameters of a low-level atmospheric jet.  $z_j$  is the height of the jet core;  $U_j$  is the wind speed in the core.

except he does not require the jets to be elevated. Almost 80% of the tether-sounding profiles that went high enough to yield an unambiguous profile showed a jet with the characteristics depicted in Figure 5.

Figure 6 shows statistics of the jets observed on ISW. In 103 available soundings, the jet core was always below 425 m; two-thirds of the jets occurred between 25 and 175 m (Figure 6a). Speeds in the core of the jet ranged between 3.0 and 13.6  $\text{m s}^{-1}$ , with a majority of the speeds being between 4 and 10  $\text{m s}^{-1}$  (Figure 6b).

Figure 7 demonstrates that the jet is truly low-level and could be considered a boundary-layer phenomenon (cf. Beyrich and Klose, 1988). For only seven of the 82 observed jets was the core of the jet above the top of the temperature inversion layer. In other words, the jets were usually embedded in the inversion layer. While the inversion height  $z_t$  is often taken as the nominal height of the ABL, we will explain shortly that, for SBLs,  $z_t$  usually overestimates the boundary-layer height.

Low-level jets are commonly found in nocturnal boundary layers at lower latitudes (e.g., Blackadar, 1957; Bonner, 1968; Stull, 1988, p. 520 ff.; Kurzeja et al., 1991; Singh et al., 1993; Mahrt, 1999). Zemba and Friehe (1987), Smedman et al. (1997), and Källstrand (1998) also observed jets during daytime in stably stratified ABLs over water. In a setting similar to ours, Walter and Overland (1991) found low-level jets over sea-ice in the central Arctic during two days of aircraft observations.

Several processes are known to cause low-level jets; Stull (1988, p. 521 ff.) listed most of these. For example, Bonner (1968) suggested that the low-level jet

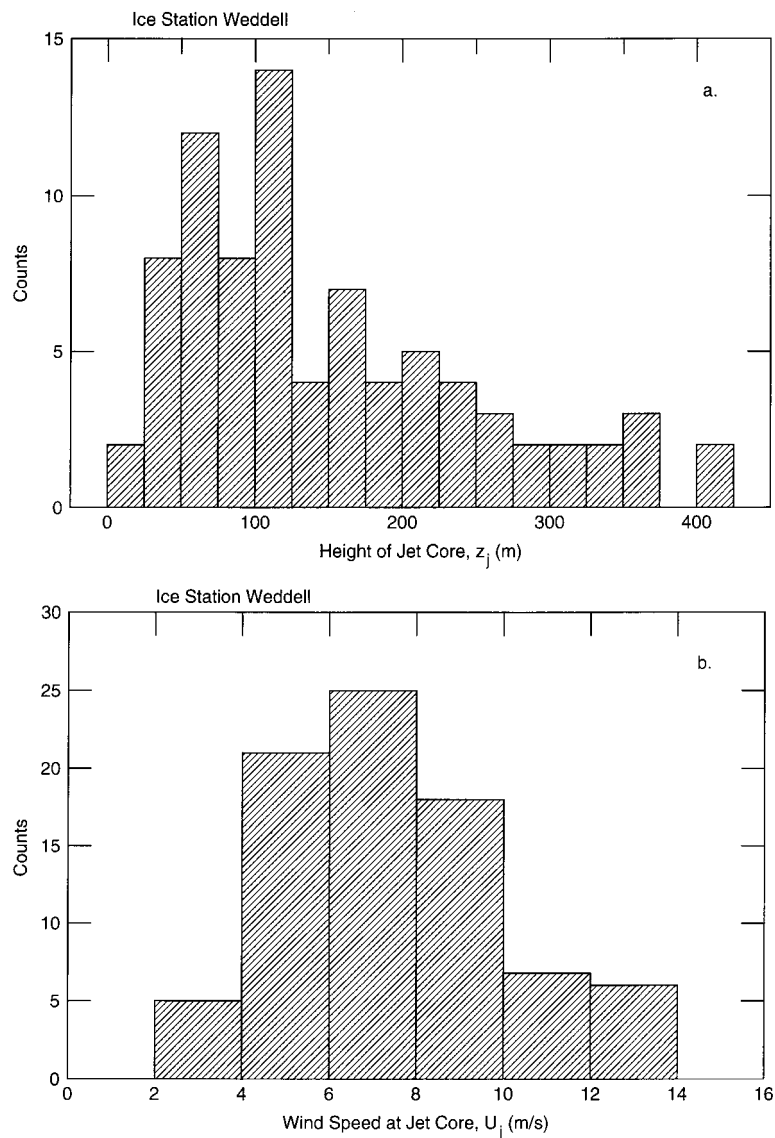


Figure 6. Histograms of low-level jet statistics as observed on Ice Station Weddell. Panel a shows the height of the jet core ( $z_j$ ), while panel b shows the wind speed in the core ( $U_j$ ).

frequently seen over the U.S. Great Plains results from baroclinicity induced, either thermally or dynamically, by the Rocky Mountains. Zemba and Friehe (1987) also showed that the jet they observed off the California coast resulted from the baroclinicity caused by the land-sea surface temperature difference. Frequently, jets are presumed to be manifestations of inertial oscillations in a layer decoupled from the surface by frictional damping (e.g., Blackadar, 1957; Thorpe and Guymer, 1977;

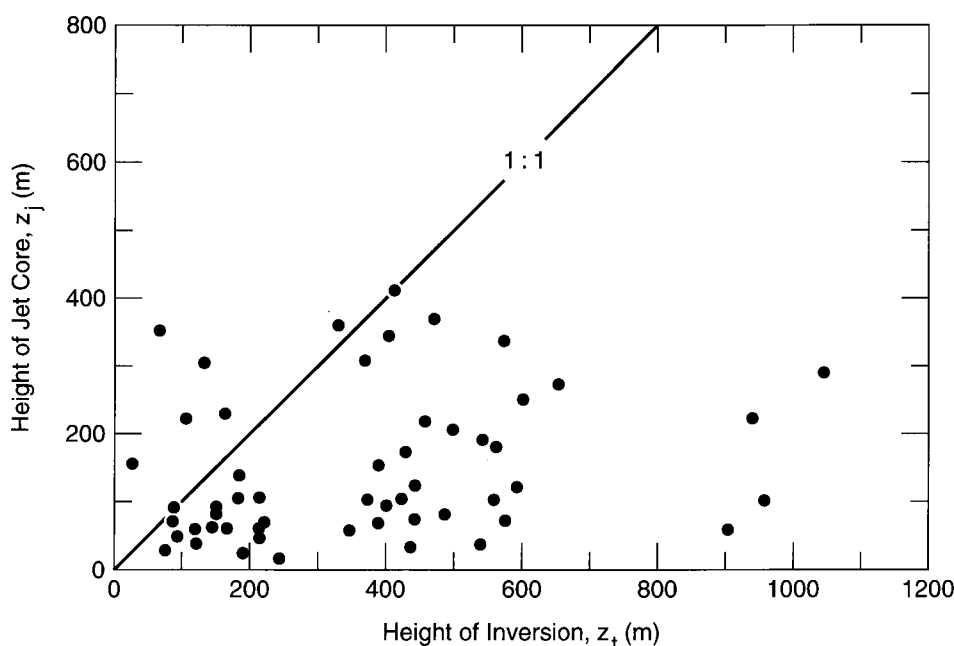


Figure 7. A comparison of the height of the jet core,  $z_j$ , with the height of the top of the low-level temperature inversion,  $z_t$ . The 1 : 1 line shows where the two heights are equal.

Smedman et al., 1993; Källstrand, 1998; Mahrt, 1999). In the Antarctic specifically, jets have been associated with katabatic winds (King and Turner, 1997, p. 296 ff.) and with the barrier winds blowing northward on the east side of the Antarctic Peninsula (Parish, 1983; Schwerdtfeger, 1984, p. 78 ff.; King and Turner, 1997, p. 281 ff.).

As we have mentioned, our site was ideal for an SBL experiment. ISW was always at least 200 km from the nearest topography; there was no surface slope; and the surface was covered in sea-ice (with, perhaps, 5% lead coverage) and, thus, was fairly homogeneous for several hundred kilometres in all directions. As a result, we can discard some of the explanations in Stull's (1988, p. 521 ff.) list of causes for low-level jets as not relevant to our setting. The data that we collected on ISW also argue against some of the explanations.

For example, Figure 8 shows the direction toward which the wind was blowing in the core of the observed jets. The ISW jets blew in all directions, with north and northeast and south and southwest orientations represented most. The wide angular distribution of these jet directions argues against topographic or surface control of the jets. If baroclinicity resulting from the surface temperature contrast between the ice-covered Weddell Sea and the open ocean to the north and east caused the jets, their preferred direction would be southeasterly (e.g., Andreas, 1998) since the nearest ice edge generally runs north-south or northwest-southeast in February, March, April, and May (Zwally et al., 1983; Gloersen et al., 1992).

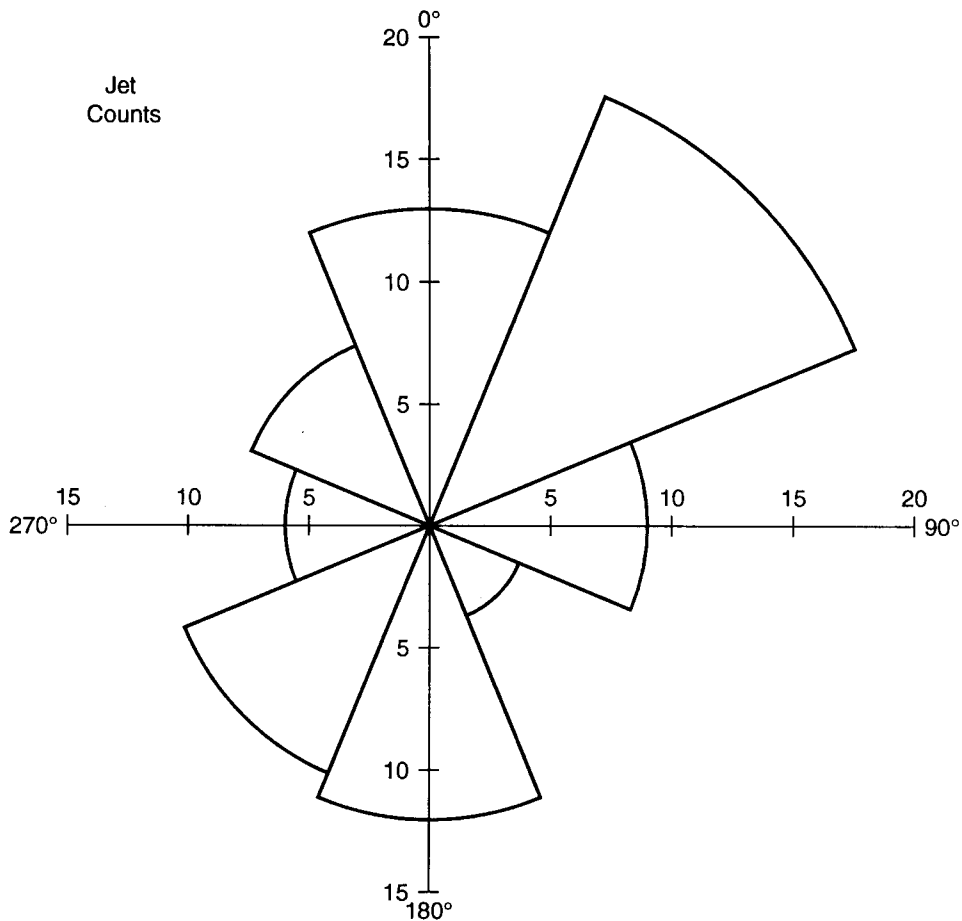


Figure 8. Histogram of the direction toward which the wind was blowing in the core of the observed jets. Each sector is  $45^\circ$  wide; the radius of the sector indicates the number of jets within that angle interval.

Thus, baroclinicity arising from a gradient in surface temperature might explain some, but by no means all, of the observed jets.

Likewise, the barrier winds east of the mountains of the Antarctic Peninsula parallel the mountains with the mountains on their left. That is, the jet in the barrier winds blows strictly toward the north. In addition, Parish's (1983) model and the scale analysis by King and Turner (1997, p. 283) suggest that, since ISW was at least 300 km from the foot of the mountains, it was generally beyond the region influenced by these barrier winds. And, according to Parish's model, ISW was an order of magnitude beyond the region where the jet in the barrier wind occurs. Consequently, it is unlikely that the observed jets resulted from topographic effects.

The turning angle of the wind in the radiosonde profile gives us other clues about the dynamics of the jet. Figure 9 shows the angular separation between the

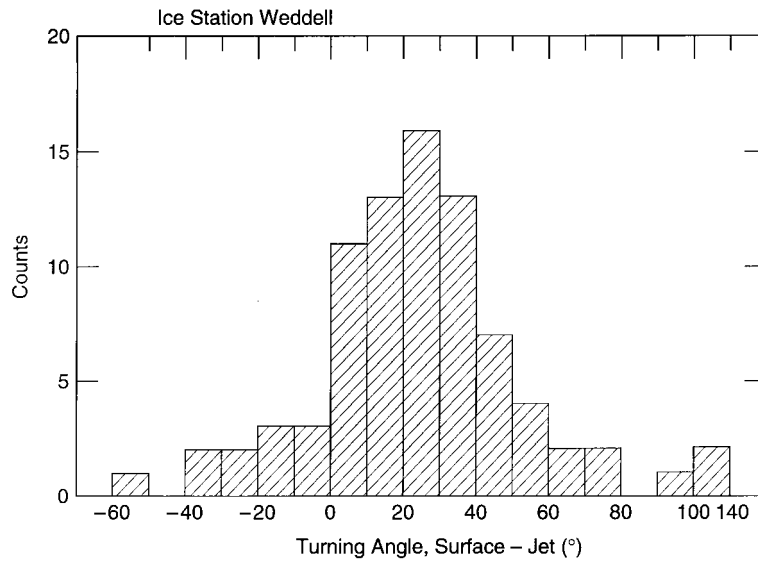


Figure 9. Histogram of the turning angle of the jet. This shows the difference in direction between the wind vector at the surface and in the core of the jet, where positive angles denote counterclockwise rotation with height.

wind vector in the core of the jet and at the surface. In the figure, positive angles mean that the jet is counterclockwise from the surface wind when viewed from above. The few large or outlying angles in the figure may be real but most likely result from scatter in the single-level radiosonde wind data.

Because most of the angles in Figure 9 are positive, the turning of the jet with respect to the surface wind seems to be controlled by Ekman dynamics (e.g., Brown, 1990; Andreas, 1998). The distribution of observed turning angles also suggests that the direction of the jet is related to the direction of the geostrophic wind (e.g., Overland and Davidson, 1992; Overland and Colony, 1994).

In summary, by virtue of our setting and our observations, we can easily discount most of the mechanisms typically cited as causing low-level jets. In light of Figure 9, we henceforth focus on the remaining, plausible explanation for our observed jets: inertial oscillations in a layer decoupled from the surface by the stable stratification.

#### 4. Model of the Low-Level Jet

##### 4.1. THORPE AND GUYMER'S MODEL

We will use a model presented by Thorpe and Guymer (1977) to evaluate whether such inertial oscillations can explain our observations. Thorpe and Guymer actually presented models for both convective daytime and stable nocturnal boundary

layers. Because we saw predominantly stable stratification and no convection, however, we use only their model of the nocturnal boundary layer. This builds on Blackadar's (1957) model in which an elevated layer becomes frictionally decoupled from a lower layer because the stable stratification has eliminated turbulent exchange between the layers. When this decoupling occurs, the upper layer begins inertial oscillations that lead to frequent supergeostrophic speeds in the layer. Malcher and Kraus (1983) and Beyrich and Klose (1988) also based models of the low-level jet on Thorpe and Guymer's work.

Thorpe and Guymer's (1977) nocturnal boundary-layer model has two layers. The lower layer, which has thickness  $h$ , is frictionally coupled to the surface by turbulent momentum exchange. It is basically an Ekman layer in which the layer-averaged easterly ( $U$ ) and northerly ( $V$ ) velocity components obey

$$\frac{dU}{dt} - fV = \frac{1}{\rho} \frac{d\tau_x}{dz}, \quad (1a)$$

$$\frac{dV}{dt} + f(U - U_g) = \frac{1}{\rho} \frac{d\tau_y}{dz}. \quad (1b)$$

Here,  $t$  is time,  $z$  is height,  $f$  is the Coriolis parameter,  $U_g$  is the easterly component of the geostrophic wind (the northerly component,  $V_g$ , is taken as zero),  $\rho$  is the (constant) air density, and  $\tau_x$  and  $\tau_y$  are the easterly and northerly components of the horizontal stress.

The stable stratification has damped out the turbulence above height  $h$ . Consequently, in the upper layer, we find only inertial oscillations governed by

$$\frac{dU}{dt} - fV = 0, \quad (2a)$$

$$\frac{dV}{dt} + f(U - U_g) = 0. \quad (2b)$$

Thorpe and Guymer (1977) included only two layers in their model of the nocturnal boundary layer: the lower turbulent layer, which reaches height  $h$ , and the upper nonturbulent layer that extends up to height  $h_u$ , which is associated with the top of the inversion layer  $z_t$ . Mahrt et al. (1979), however, explained that the region immediately above the jet is intermittently turbulent because of the wind shear. This turbulence extracts energy from the mean wind and, thus, accentuates the jet profile. In other words, this intermittently turbulent layer is crucial for producing a jet with the features depicted in Figure 5 (cf. Makshtas et al., 1998). Above this intermittently turbulent layer, we assume geostrophic balance.

Figure 10 is a histogram of inferred values of the geostrophic wind speed  $G$  [ $= (U_g^2 + V_g^2)^{1/2}$ ] associated with our jet profiles. Plotted values are simply the tethered-sonde measurements of wind speed in the region above the jet. Källstrand (1998) found that similar estimates of the geostrophic wind speed obtained from

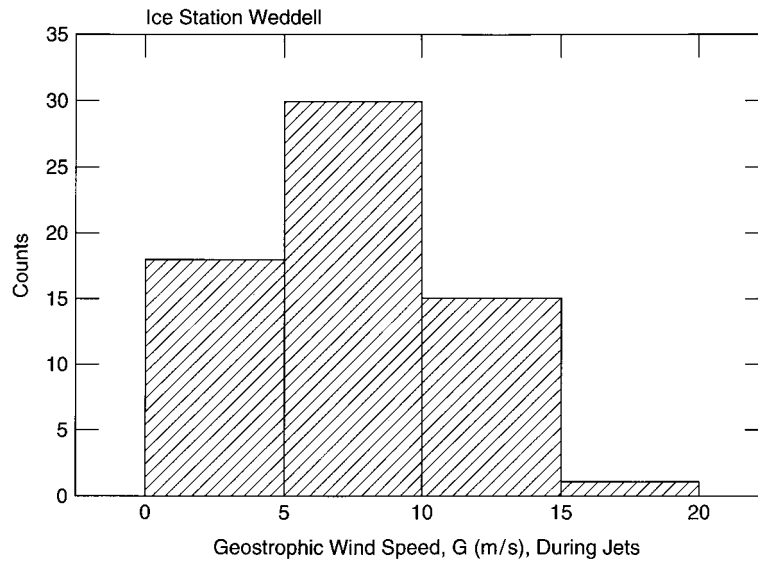


Figure 10. Histogram of the geostrophic wind speed ( $G$ ) inferred from the radiosonde profiles that showed low-level jets.

pibals agreed reasonably well with estimates based on the surface pressure field. Nevertheless, we consider the values in Figure 10 to be suggestive rather than precise and, therefore, use wider histogram bars than in Figure 6b, for example. (Figure 10 does not contain 82 observations because, again, though our soundings went high enough to capture a jet, they did not always go high enough for us to evaluate a representative geostrophic wind speed above the jet.)

To start the nocturnal evolution of their model, Thorpe and Guymer (1977) assumed that, at time zero, the lower and upper model layers were moving as one layer with uniform velocity, the components of which were  $U_0$  and  $V_0$ . At time zero, this well-mixed layer collapses, and the upper layer instantaneously becomes frictionally decoupled from the lower layer and begins undamped inertial oscillations. With these initial conditions, the wind vector in the upper model layer has the analytical solution

$$U(t) = (U_0 - U_g) \cos(ft) + V_0 \sin(ft) + U_g, \quad (3a)$$

$$V(t) = V_0 \cos(ft) - (U_0 - U_g) \sin(ft). \quad (3b)$$

This is the same solution for the upper layer that Blackadar (1957) derived.

Since our observations on ISW did not show the daily growth and collapse of a mixed layer that Thorpe and Guymer (1977) assumed, we can only speculate on what triggers the inertial oscillations. On ISW, we continuously measured surface-level profiles of temperature and wind speed on fixed masts (Andreas et al., 1992; Makshtas et al., 1999). From these data, we used Monin–Obukhov similarity theory

to compute hourly averages of the surface fluxes of momentum and sensible heat and the Obukhov length  $L$ , which characterizes the stability of the atmospheric surface layer (ASL). Although the ABL was virtually always stably stratified, the ASL was occasionally unstably stratified according to these calculations. Using  $L$  as the criterion, we found that, between March 1 and June 4 on ISW, there were eight episodes of unstable or near-neutral stratification in the ASL that lasted at least one day and four episodes that lasted at least three days. Of the 18 tethered sondes soundings between March 1 and June 4 that revealed no low-level jet, eight were made during or shortly after these periods of unstable stratification in the ASL.

In summary, we presume, as did Thorpe and Guymer (1977), that the onset of stable stratification in the ABL triggers the low-level jets. Day-long periods of unstable stratification in the atmospheric surface layer, probably associated with advective events, can foster sufficient mixing within the ABL to erode the jet. An obvious, related conclusion is that, when once triggered, the inertial oscillations are long lasting since we saw them in 80% of the soundings.

To treat the evolution of the lower layer, Thorpe and Guymer (1977) assumed that the stress profile in Equation (1) is linear. That is,

$$\tau_x = \tau_{xs} \left(1 - \frac{z}{h}\right), \quad (4a)$$

$$\tau_y = \tau_{ys} \left(1 - \frac{z}{h}\right), \quad (4b)$$

where  $\tau_{xs}$  and  $\tau_{ys}$  are surface values of the respective stress components. Overland (1985) corroborated this assumption by showing several stress profiles measured over Arctic sea-ice that were approximately linear with height. Nicholls (1985) also reported an approximately linear stress profile in a well-mixed boundary layer over water. The stress data that Caughey et al. (1979) obtained under stable stratification during the Minnesota experiment also are compatible with a linear decrease in stress with height. As a counterpoint, though, Smedman's (1991) observations in SBLs seem to follow

$$\tau = \tau_s \left(1 - \frac{z}{h}\right)^{7/4}, \quad (5)$$

where  $\tau = (\tau_x^2 + \tau_y^2)^{1/2}$  and  $\tau_s = (\tau_{xs}^2 + \tau_{ys}^2)^{1/2}$ .

Although this issue about the form of the stress profile is, thus, still unresolved, we assume that the stress profile is linear because this form greatly simplifies the analysis. With Equation (4) substituted into Equation (1),

$$\frac{dU}{dt} - fV = -\frac{\tau_{xs}}{\rho h}, \quad (6a)$$

$$\frac{dV}{dt} + f(U - U_g) = -\frac{\tau_{ys}}{\rho h}. \quad (6b)$$

Thorpe and Guymer (1977) offered two solutions to this set of equations: the first uses a parameterization for the surface stress that is linear in wind speed; the second uses a parameterization that is quadratic in wind speed. We discuss only the quadratic parameterization since no known observations support the validity of a shear stress parameterization that depends linearly on wind speed.

#### 4.2. QUADRATIC STRESS RELATION

Thorpe and Guymer's (1977) model of the wind vector in the lower layer based on a quadratic stress relation parameterizes the surface stress as

$$\tau_{xs} = \rho C_D (U^2 + V^2)^{1/2} U, \quad (7a)$$

$$\tau_{ys} = \rho C_D (U^2 + V^2)^{1/2} V, \quad (7b)$$

where  $C_D$  is the drag coefficient. Substituting Equation (7) into Equation (6) yields equations for the velocity components in the lower layer:

$$\frac{dU}{dt} = fV - C_D (U^2 + V^2) U / h, \quad (8a)$$

$$\frac{dV}{dt} = -f(U - U_g) - C_D (U^2 + V^2)^{1/2} V / h. \quad (8b)$$

We solved these equations for the velocity components in the lower layer using the fourth-order Runge–Kutta formula (e.g., Press et al., 1994, p. 702 ff.). For  $C_D$ , we used the average value for the 10-m, neutral-stability drag coefficient,  $C_{DN10}$ , that Andreas and Claffey (1995) measured on ISW,  $1.9 \times 10^{-3}$ . Equation (3) gives the solution in the upper layer.

Figure 11 shows wind hodographs in the lower and upper model layers, computed with Equation (8) and Equation (3), respectively, for typical ISW values of latitude, jet height  $h$  (Figure 7), and geostrophic wind speed  $G$  (Figure 10). At time zero, when the upper layer becomes frictionally decoupled from the surface, it begins undamped inertial oscillations about the geostrophic wind vector. The velocity vector in the lower layer rapidly decays and turns clockwise (in the Southern Hemisphere), reaching steady state in about five hours.

Let us look more closely at the steady-state behaviour of the wind vectors in the upper and lower layers. Equation (3) represents a vector from the origin that terminates on a circle of radius

$$R = [(U_0 - G)^2 + V_0^2]^{1/2}, \quad (9)$$

centered on the geostrophic wind vector. The tip of the wind vector in the upper layer makes one complete cycle around this circle for each inertial period starting at time zero. As a result, the angular deviation between the wind vector in the upper



where  $S_Q$  is the magnitude of the steady-state wind vector in the lower layer,

$$S_Q^2 = U^2(t \rightarrow \infty) + V^2(t \rightarrow \infty) = \frac{f^2 h^2}{2C_D^2} \left[ \left( 1 + \frac{4GC_D^2}{f^2 h^2} \right)^{1/2} - 1 \right]. \quad (13)$$

The subscript  $Q$  reminds us that this result derives from Thorpe and Guymer's (1977) quadratic stress parameterization.

The angular separation between the geostrophic wind vector and the steady-state wind vector in the lower layer is

$$\begin{aligned} \alpha_Q &= -\arctan \left( \frac{C_D S_Q}{fh} \right) \\ &= -\arctan \left\{ \text{sign } f \left[ \frac{1}{2} \left( 1 + \frac{4GC_D^2}{f^2 h^2} \right)^{1/2} - \frac{1}{2} \right]^{1/2} \right\}. \end{aligned} \quad (14)$$

Here  $\text{sign } f$  represents the sign of the Coriolis parameter, and the minus sign in front of the right two terms transforms our Cartesian model coordinates into a meteorological coordinate system in which angles increase clockwise. Thus, positive  $\alpha_Q$  means that the steady-state wind in the lower layer is clockwise from the geostrophic wind when viewed from above. (Remember,  $f$  is negative in the Southern Hemisphere.)

From Equation (10) and Equation (14), we deduce that, in steady state, the angular deviation between the wind vector in the jet and in the lower layer is bounded by  $|\alpha_Q \pm \beta|$ . For the example in Figure 11,  $\alpha_Q = 57^\circ$  and  $\beta = 24^\circ$ . Consequently, for the typical ISW conditions depicted in Figure 11, we would expect to see turning angles between the jet and the surface wind ranging from  $33^\circ$  to  $81^\circ$ . Figure 9 shows that this prediction agrees fairly well with our ISW observations.

It is also easy to determine geometrically from Figure 11 how frequently jets should be observed if our model is accurate. The steady-state wind vector in the lower layer has magnitude  $S_Q$  of  $5.45 \text{ m s}^{-1}$ . Thus, we simply inscribe an arc with radius  $S_Q + 2 \text{ m s}^{-1}$  ( $= 7.45 \text{ m s}^{-1}$ ) around the origin in Figure 11. Any segment of the wind hodograph in the upper layer that is inside this circle would not produce a jet profile according to our definition. Segments of the hodograph outside this circle, on the other hand, have a wind speed that is at least  $2 \text{ m s}^{-1}$  higher than the speed in the lower layer and would produce a jet profile. Approximately  $10/13 = 77\%$  of the upper-level hodograph is outside this circle of radius  $7.45 \text{ m s}^{-1}$ . This percentage agrees remarkably well with our ISW result that 80% of available tethersonde profiles showed a low-level jet.

Lastly, according to Figure 11, the range of speeds in the modelled jet is  $7.4$  to  $14 \text{ m s}^{-1}$ . Our observations (Figure 6b) yielded some jets with core speeds less than  $6 \text{ m s}^{-1}$ , but most speeds were between  $6$  and  $14 \text{ m s}^{-1}$ , as Figure 11 predicts.

Ultimately, this range of speeds depends mostly on the speed of the geostrophic wind.

In summary, the Thorpe and Guymer (1977) model of low-level jets, based on undamped inertial oscillations in an elevated layer that is frictionally decoupled from the surface, does well in explaining the range of observations we made in low-level jets on ISW. In particular, model calculations predict both the correct percentage of jet occurrences and the range of angular deviations between the surface wind vector and the wind vector in the jet core. Our modelling, of course, does not rule out other causes of the jets but suggests that the modelled scenario is the dominant one in the western Weddell Sea in autumn and early winter.

## 5. Discussion

### 5.1. BOUNDARY-LAYER HEIGHT

For the model calculations in the last section, we took the height  $h$  to be the height of the jet core. For a convective boundary layer, the height of the inversion  $z_t$  is commonly used as the ABL height (e.g., Kaimal et al., 1976). For the SBL, however, this height is not as meaningful. Mahrt (1981) and Zilitinkevich and Mironov (1996), for example, explained that, in stable stratification, the ABL should be defined as the region that is at least intermittently turbulent. We infer that the SBL is thus the region between the surface and the core of the low-level jet. Figure 7 emphasizes that, with this definition, the height of the SBL is usually much less than  $z_t$ .

The Richardson number helps us decide where turbulence is present. Mahrt (1981) and Heinemann and Rose (1990) defined a bulk Richardson number from radiosounding data as

$$\text{Ri}(z) = \frac{gz}{\Theta(z)} \frac{\Theta(z) - \Theta_s}{S^2(z)}. \quad (15)$$

Here,  $g$  is the acceleration of gravity;  $z$ , the height of a radiosounding observation;  $\Theta(z)$  and  $S(z)$ , the potential temperature and wind speed at  $z$ ; and  $\Theta_s$ , the potential temperature at the surface (which we computed from the temperature at the lowest radiosounding level, about 2 m).

As we scan up a radiosounding profile, computing  $\text{Ri}(z)$  at each reporting height  $z$ , we compare  $\text{Ri}(z)$  with the critical Richardson number  $\text{Ri}_{cr}$ , where  $\text{Ri}_{cr} = 0.4$ , a value midway between Mahrt's (1981) 0.5 and Heinemann and Rose's (1990) 0.33. If  $\text{Ri}(z) < \text{Ri}_{cr}$ , we assume that the layer between the surface and height  $z$  is turbulent and, thus, that level  $z$  is still within the boundary layer. The lowest level for which  $\text{Ri}(z) \geq \text{Ri}_{cr}$  is denoted  $z_{\text{Ri}}$  and is assumed to be the top of the turbulent region. That is,  $z_{\text{Ri}}$  estimates the height of the SBL.

Figure 12 shows time series of our observations of  $z_t$  and  $z_j$  and our computed  $z_{Ri}$  values. Although the  $z_j$  and  $z_{Ri}$  points in panel b do not track perfectly,  $z_j$  is much more closely related to  $z_{Ri}$  than it is to  $z_t$ . On average,  $z_j$  and  $z_{Ri}$  agree very well. The average of the  $z_j$  values in Figure 12 is 151 m; the average of the  $z_{Ri}$  values is 143 m. Hence, as Mahrt (1981) concluded, the height of the low-level jet is an indicator of the height of the SBL. Therefore, we can approximate the height  $h$  of the lower layer in the model described in the last section with either  $z_j$  or  $z_{Ri}$ , whichever is more readily available.

Makshtas et al. (1998) attributed the ranges of  $z_j$  and  $z_{Ri}$  in Figures 7 and 12 to the influence of the surface radiation balance on boundary layer turbulence. Figure 12 also shows the time series of daily averaged net radiation,  $R_n$ , that we measured on ISW with individual radiometers that monitored incoming and outgoing longwave and shortwave radiation (Andreas et al., 1992; Makshtas et al., 1999). Our convention is that  $R_n$  is positive when the surface is gaining energy radiatively. A negative net radiation means that the surface is losing energy radiatively; this would lead to stable stratification.

Although the correlation between  $R_n$  and any of the heights plotted in Figure 12,  $z_t$ ,  $z_j$ , or  $z_{Ri}$ , is not high, the plot is suggestive. When  $R_n$  is positive or near zero,  $z_t$ ,  $z_j$ , and  $z_{Ri}$  all tend to be larger than when  $R_n$  is more negative. When the radiative losses become large, i.e., when the hourly values are about  $-40 \text{ W m}^{-2}$ , internal gravity waves begin breaking within the boundary layer and create new turbulence (Makshtas et al., 1998). Thus, the height of the SBL reaches a quasi-minimum of 50–100 m with strong radiative forcing.

## 5.2. GEOSTROPHIC DRAG COEFFICIENT

In large-scale sea-ice and ocean models, it is common to estimate the surface stress  $\tau$  with a geostrophic drag relation

$$\tau = \rho C_g^2 G^2, \quad (16)$$

where  $C_g$  is the geostrophic drag coefficient, and  $G$  is again the geostrophic wind speed (e.g., Parkinson and Washington, 1979; Brown and Liu, 1982; Hibler, 1985; Overland and Davidson, 1992; Brown and Foster, 1994). Often  $C_g$  is taken as a constant; but, in general, it depends on boundary-layer characteristics such as stability, surface roughness, or ABL height (e.g., Overland and Davidson, 1992; Overland and Colony, 1994; Brown and Foster, 1994; Andreas, 1998).

The turning angle  $\alpha$  between the geostrophic wind vector and the surface wind vector is the second piece of information needed to specify surface stress from the geostrophic wind. Again, some assume that  $\alpha$  is constant; but, in general, it also depends on ABL characteristics.

The jet model we described in Section 4 implies a new geostrophic drag relation appropriate when low-level jets are present. Although Thorpe and Guymmer (1977)

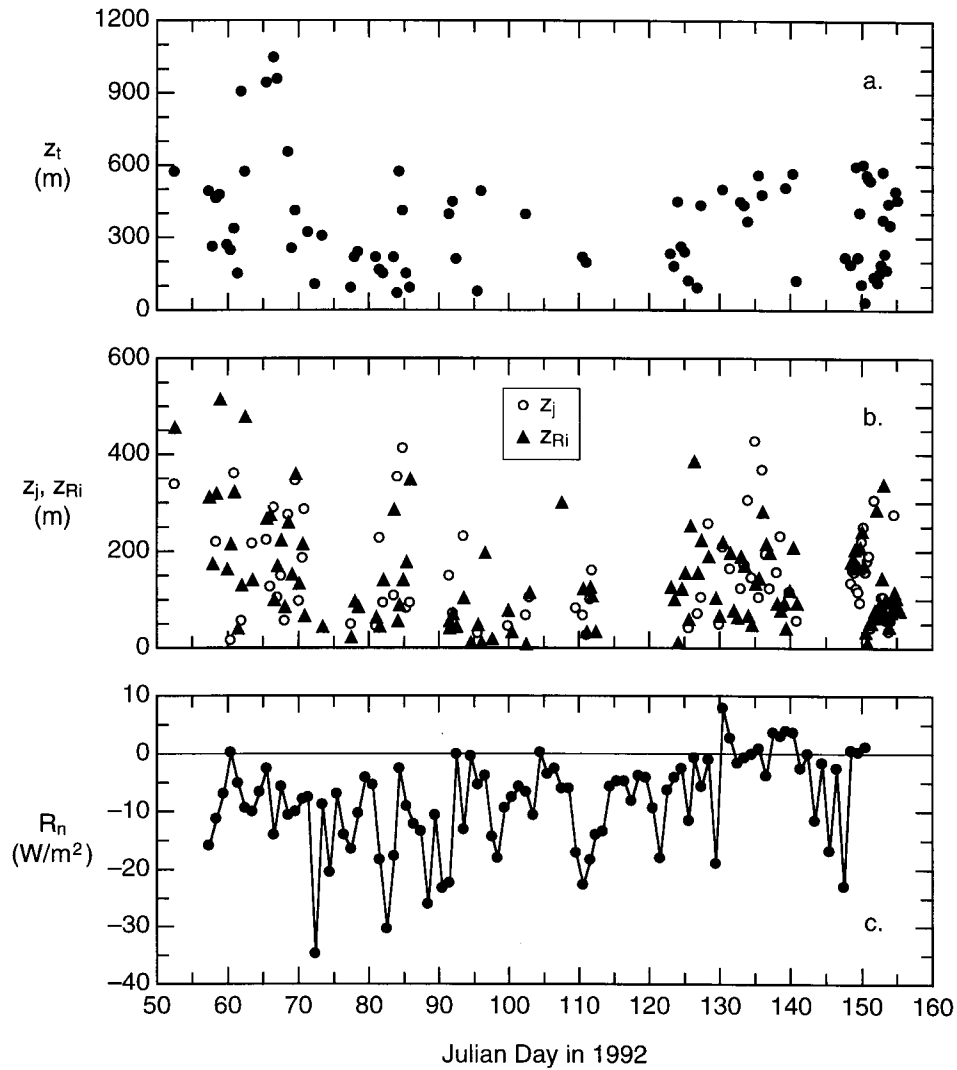


Figure 12. Ice Station Weddell observations of inversion height ( $z_t$ ; panel a) and height of the jet core ( $z_j$ ; panel b) based on radiosounding data. Panel b also shows the height of the stable boundary layer ( $z_{Ri}$ ) estimated from a critical Richardson number criterion. Panel c shows the daily averaged net radiation ( $R_n$ ) on ISW.

developed this jet model, they did not discuss the geostrophic drag relation implied by it.

The quadratic stress relation, Equation (7), gives

$$\tau = \rho C_D (U^2 + V^2), \quad (17)$$

which at steady-state is

$$\tau = \rho C_D S_Q^2. \quad (18)$$

Combining this with Equation (16) yields

$$C_g = \frac{C_D^{1/2} S_Q}{G}. \quad (19)$$

In turn, substituting (13) here gives

$$C_g = \frac{|f|h}{\sqrt{2}C_D^{1/2}G} \left[ \left( 1 + \frac{4G^2C_D^2}{f^2h^2} \right)^{1/2} - 1 \right]^{1/2}, \quad (20)$$

while Equation (14) gives the turning angle  $\alpha$  between the geostrophic wind and the surface stress vector. In a meteorological coordinate system, we simply add  $\alpha$  to the direction of the geostrophic wind to find the direction of the surface stress.

Note that, because our model treats only the SBL when jets are present, neither Equation (20) nor the expression for the turning angle (14) contains any explicit stability dependence. Such stability dependence is usual in expressions that model the geostrophic drag coefficient for general conditions (e.g., Brown, 1990; Overland and Colony, 1994; Andreas, 1998).

Figure 13 shows  $C_g$  and  $\alpha$  for conditions typical of ISW, as predicted by Equations (14) and (20). Despite the absence of any stability dependence in our model, for values of  $G$ ,  $h$ , and  $C_{DN10}$  that we observed on ISW, the predicted  $C_g$  and  $\alpha$  values still span the range of values obtained from observations over Arctic sea-ice (e.g., Brown, 1981; Overland, 1985; Overland and Davidson, 1992; Overland and Colony, 1994). That is, variations in  $G$ ,  $h$ , and  $C_{DN10}$  provide enough degrees of freedom for our jet model to produce all observed values of  $C_g$  and  $\alpha$  without the need for an additional, independent stratification parameter. Overland and Davidson (1992) and Overland and Colony (1994), in contrast, predicted  $C_g$  and  $\alpha$  on the basis of stratification alone and included no explicit dependence on  $G$ ,  $h$ , or  $C_{DN10}$ . We infer that a stratification parameter and the parameter set  $\{G, h, C_{DN10}\}$  provide redundant information for the ABL over polar sea-ice.

We can summarize Figure 13 by noting that  $C_g$  is smaller and the absolute value of  $\alpha$  is larger when the boundary-layer height  $h$  is smaller. Conversely, as  $h$  increases,  $C_g$  becomes larger and  $|\alpha|$  becomes smaller. Clearly, when viewed from above, the surface wind (and surface stress) is clockwise from the geostrophic wind in the Southern Hemisphere and counterclockwise in the Northern Hemisphere.

Our model for the geostrophic drag relation, represented by Equation (14) for  $\alpha$  and (20) for  $C_g$ , is more complex than some currently in use, for example, those that use constant values for both  $C_g$  and  $\alpha$ . But it is also less complex than some that require detailed atmospheric temperature data for computing a stratification parameter. Our model is simpler than these because it applies only over sea-ice, where the stratification is usually stable and the height of the SBL is, thus, generally constrained between 50 and 300 m.

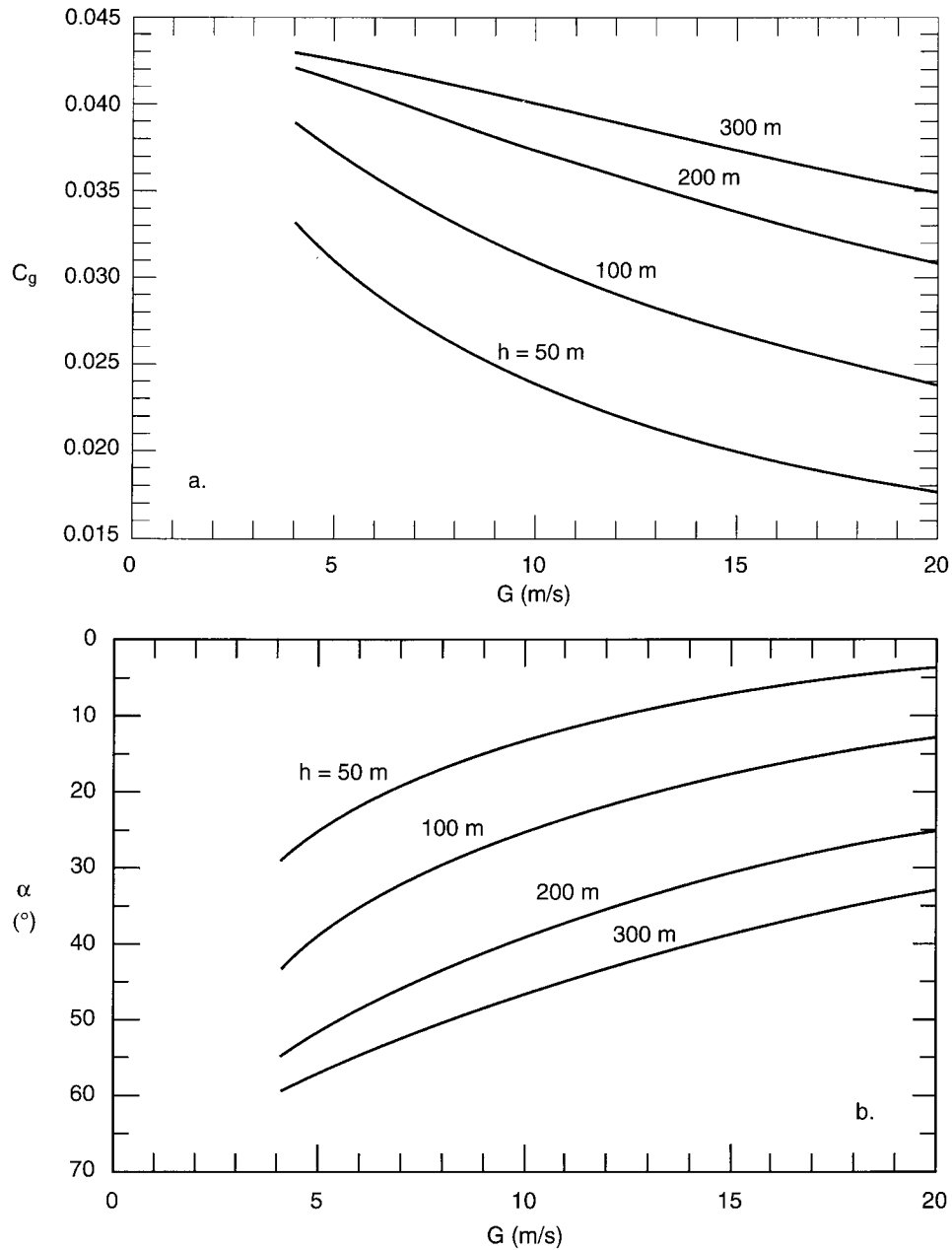


Figure 13. The geostrophic drag relation derived from the jet model. Panels a and b, respectively, show the geostrophic drag coefficient  $C_g$  (see Equation (20)) and the turning angle  $\alpha$  (see Equation (14)) between the geostrophic wind vector and the surface stress in the Southern Hemisphere as functions of the geostrophic wind speed.  $h$  is the height of the stable boundary layer. Positive  $\alpha$  values mean that the surface stress is clockwise from the geostrophic wind vector when viewed from above. Calculations assume  $C_D = C_{DN10} = 1.9 \times 10^{-3}$  and that the latitude is  $68^\circ\text{S}$ .

## 6. Conclusions

We have presented here the first long-term, detailed observations of the structure of the atmospheric boundary layer over Antarctic sea-ice. Over sea-ice, the ABL, defined as the near-surface layer that is, at least, intermittently turbulent, is often stably stratified. During four months of radiosonde observations on Ice Station Weddell in the austral autumn and early winter, we found a low-level inversion layer 96% of the time. Because statistics of these ISW inversions are grossly similar to the statistics of inversions observed in and around the Arctic Ocean, we presume that ABL characteristics over sea-ice regions in both hemispheres are largely locally controlled by the interplay among the sea-ice surface, the free atmosphere, and the clouds.

The stable stratification of ISW frequently produced low-level atmospheric jets. Eighty percent of our soundings that yielded unambiguous wind speed profiles showed a jet with its core below 425 m. A simple two-layer model, in which an elevated layer is frictionally decoupled from a near-surface layer and thus undergoes undamped inertial oscillations, can explain most of the features of the low-level jets that we have documented.

This two-layer model also implies a geostrophic drag parameterization that relates the geostrophic drag coefficient and the turning angle to latitude, ABL height, geostrophic wind speed, and the 10-m drag coefficient. Because this parameterization presupposes stable stratification and a decoupled elevated layer, it is more limited than some geostrophic drag relations; but it can consequently also be simpler. Our parameterization does not explicitly depend on a stratification parameter, as other more complex parameterizations do, and the independent variables are either readily available or have only limited domains. Because stable stratification is very common over sea-ice, this geostrophic drag parameterization may thus be widely applicable despite its simplicity.

## Acknowledgements

We dedicate this manuscript to the memory of William T. Bates, who drafted most of the figures in it. His passing left an enormous hole in CRREL's technical publishing group. We thank Larry Mahrt, John Weatherly, and two anonymous reviewers for comments on the manuscript. The U.S. National Science Foundation supported this work with grants OPP-90-24544, OPP-93-12642, OPP-97-02025, and OPP-98-14024; the U.S. Department of the Army supported it through project 4A161102AT24.

## References

- Andreas, E. L.: 1998, 'The Atmospheric Boundary Layer over Polar Marine Surfaces', in M. Leppäranta (ed.), *Physics of Ice-Covered Seas*, Vol. 2, Helsinki University Press, pp. 715–773.
- Andreas, E. L. and Cash, B. A.: 1999, 'Convective Heat Transfer over Wintertime Leads and Polynyas', *J. Geophys. Res.* **104**(C11), 25,721–25,734.
- Andreas, E. L. and Claffey, K. J.: 1995, 'Air-Sea Drag Coefficients in the Western Weddell Sea: 1. Values Deduced from Profile Measurements', *J. Geophys. Res.* **100**(C3), 4821–4831.
- Andreas, E. L. and Richter, W. A.: 1982, 'An Evaluation of Vaisala's MicroCORA Automatic Sounding System', CRREL Rept. 82-28, U.S. Army Cold Regions Research and Engineering Laboratory, Hanover, NH, 17 pp. [NTIS: AD-B070011.]
- Andreas, E. L., Claffey, K. J., Makshtas, A. P., and Ivanov, B. V.: 1992, 'Atmospheric Sciences on Ice Station Weddell', *Antarct. J. U.S.* **27**(5), 115–117.
- Andreas, E. L., Claffey, K. J., and Makshtas, A. P.: 1993, 'Low-Level Atmospheric Jets and Inversions on Ice Station Weddell 1', *Antarct. J. U.S.* **28**(5), 274–276.
- Andreas, E. L., Claffey, K. J., and Makshtas, A. P.: 1995, 'Low-Level Atmospheric Jets over the Western Weddell Sea', in Preprint Volume, Fourth Conference on Polar Meteorology and Oceanography, 15–20 January 1995, Dallas, TX, American Meteorological Society, Boston, pp. 252–257.
- Anonymous: 1992, 'U.S. and Russian Scientists Complete Historic Weddell Sea Investigation', *Antarct. J. U.S.* **27**(4), 8–11.
- Beyrich, F. and Klose, B.: 1988, 'Some Aspects of Modelling Low-Level Jets', *Boundary-Layer Meteorol.* **43**, 1–14.
- Blackadar, A. K.: 1957, 'Boundary Layer Wind Maxima and their Significance for the Growth of Nocturnal Inversions', *Bull. Amer. Meteorol. Soc.* **38**, 283–290.
- Bonner, W. D.: 1968, 'Climatology of the Low Level Jet', *Mon. Wea. Rev.* **96**, 833–850.
- Brown, R. A.: 1981, 'Modeling the Geostrophic Drag Coefficient for AIDJEX'. *J. Geophys. Res.* **86**(C3), 1989–1994.
- Brown, R. A.: 1990, 'Meteorology', in W. O. Smith, Jr. (ed.), *Polar Oceanography, Part A. Physical Science*, Academic Press, San Diego, pp. 1–46.
- Brown, R. A. and Foster, R. C.: 1994, 'On PBL Models for General Circulation Models', *Global Atmos. Ocean System* **2**, 163–183.
- Brown, R. A. and Liu, W. T.: 1982, 'An Operational Large-Scale Marine Planetary Boundary Layer Model', *J. Appl. Meteorol.* **21**, 261–269.
- Caughey, S. J., Wyngaard, J. C., and Kaimal, J. C.: 1979, 'Turbulence in the Evolving Stable Boundary Layer', *J. Atmos. Sci.* **36**, 1041–1052.
- Claffey, K. J., Andreas, E. L., and Makshtas, A. P.: 1994, 'Upper-Air Data Collected on Ice Station Weddell', Special Rept. 94-25, U.S. Army Cold Regions Research and Engineering Laboratory, Hanover, NH, 61 pp. [NTIS: AD-289707.]
- Gloersen, P., Campbell, W. J., Cavalieri, D. J., Comiso, J. C., Parkison, C. L., and Zwally, H. J.: 1992, *Arctic and Antarctic Sea Ice, 1978–1987: Satellite Passive-Microwave Observations and Analysis*, NASA SP-511, National Aeronautics and Space Administration, Washington, D.C., 290 pp.
- Heinemann, G. and Rose, L.: 1990, 'Surface Energy Balance, Parameterizations of Boundary-Layer Heights and the Application of Resistance Laws near an Antarctic Ice Shelf Front', *Boundary-Layer Meteorol.* **51**, 123–158.
- Hibler, W. D., III: 1985, 'Modeling Sea-Ice Dynamics', *Adv. Geophys.* **28A**, 549–579.
- ISW Group: 1993, 'Weddell Sea Exploration from Ice Station', *Eos, Trans. Amer. Geophys. Union* **74**, 121–126.
- Kahl, J. D.: 1990, 'Characteristics of the Low-Level Temperature Inversion along the Alaskan Arctic Coast', *Int. J. Climatol.* **10**, 537–548.

- Kaimal, J. C., Wyngaard, J. C., Haugen, D. A., Coté, O. R., Izumi, Y., Caughey, S. J., and Readings, C. J.: 1976, 'Turbulence Structure in the Convective Boundary Layer', *J. Atmos. Sci.* **33**, 2152–2169.
- Källstrand, B.: 1998, 'Low Level Jets in a Marine Boundary Layer during Spring', *Contr. Atmos. Phys.* **71**, 359–373.
- King, J. C. and Turner, J.: 1997, *Antarctic Meteorology and Climatology*, Cambridge University Press, Cambridge, U.K., 409 pp.
- Kurzeja, R. J., Berman, S., and Weber, A. H.: 1991, 'A Climatological Study of the Nocturnal Planetary Boundary Layer', *Boundary-Layer Meteorol.* **54**, 105–128.
- Lettau, H.: 1971, 'Antarctic Atmosphere as a Test Tube for Meteorological Theories', in L. O. Quam (ed.), *Research in the Antarctic*, Pub. No. 93, American Association for the Advancement of Science, Washington, D.C., pp. 443–475.
- Mahesh, A., Walden, V. P., and Warren, S. G.: 1997, 'Radiosonde Temperature Measurements in Strong Inversions: Correction for Thermal Lag Based on an Experiment at the South Pole', *J. Atmos. Oceanic Technol.* **14**, 45–53.
- Mahrt, L.: 1981, 'Modelling the Depth of the Stable Boundary-Layer', *Boundary-Layer Meteorol.* **21**, 3–19.
- Mahrt, L.: 1999, 'Stratified Atmospheric Boundary Layers', *Boundary-Layer Meteorol.* **90**, 375–396.
- Mahrt, L., Heald, R. C., Lenschow, D. H., Stankov, B. B., and Troen, I.: 1979, 'An Observational Study of the Structure of the Nocturnal Boundary Layer', *Boundary-Layer Meteorol.* **17**, 247–264.
- Makshtas, A. P., Andreas, E. L., Svyashchennikov, P. N., and Timachev, V. F.: 1999, 'Accounting for Clouds in Sea Ice Models', *Atmos. Res.* **52**, 77–113.
- Makshtas, A. P., Timachev, V. F., and Andreas, E. L.: 1998, 'Structure of the Lower Atmospheric Layer over Ice Cover of the Weddell Sea', *Russian Meteorol. Hydrol.* **10**, 68–75.
- Malcher, J. and Kraus, H.: 1983, 'Low-Level Jet Phenomena Described by an Integrated Dynamical PBL Model', *Boundary-Layer Meteorol.* **27**, 327–343.
- Nicholls, S.: 1985, 'Aircraft Observations of the Ekman Layer during the Joint Air-Sea Interaction Experiment', *Quart. J. Roy. Meteorol. Soc.* **111**, 391–426.
- Nieuwstadt, F. T. M. and Duynkerke, P. G.: 1996, 'Turbulence in the Atmospheric Boundary Layer', *Atmos. Res.* **40**, 111–142.
- Overland, J. E.: 1985, 'Atmospheric Boundary Layer Structure and Drag Coefficients over Sea Ice', *J. Geophys. Res.* **90**(C5), 9029–9049.
- Overland, J. E. and Colony, R. L.: 1994, 'Geostrophic Drag Coefficients for the Central Arctic Derived from Soviet Drifting Station Data', *Tellus* **46A**, 75–85.
- Overland, J. E. and Davidson, K. L.: 1992, 'Geostrophic Drag Coefficients over Sea Ice', *Tellus* **44A**, 54–66.
- Parish, T. R.: 1983, 'The Influence of the Antarctic Peninsula on the Wind Field over the Western Weddell Sea', *J. Geophys. Res.* **88**(C4), 2684–2692.
- Parkinson, C. L. and Washington, W. M.: 1979, 'A Large-Scale Numerical Model of Sea Ice', *J. Geophys. Res.* **84**(C1), 311–337.
- Press, W. H., Teukolsky, S. A., Vetterling, W. T., and Flannery, B. P.: 1994, *Numerical Recipes in FORTRAN: The Art of Scientific Computing*, Second Edition, Cambridge University Press, Cambridge, U.K., 963 pp.
- Schwerdtfeger, W.: 1984, *Weather and Climate of the Antarctic*, Elsevier, Amsterdam, 261 pp.
- Serreze, M. C., Kahl, J. D., and Schnell, R. C.: 1992, 'Low-Level Temperature Inversions of the Eurasian Arctic and Comparisons with Soviet Drifting Station Data', *J. Climate* **5**, 615–629.
- Singh, M. P., McNider, R. T., and Lin, J. T.: 1993, 'An Analytical Study of Diurnal Wind-Structure Variations in the Boundary Layer and the Low-Level Nocturnal Jet', *Boundary-Layer Meteorol.* **63**, 397–423.

- Skony, S. M., Kahl, J. D. W., and Zaitseva, N. A.: 1994, 'Differences between Radiosonde and Dropsonde Temperature Profiles over the Arctic Ocean', *J. Atmos. Oceanic Technol.* **11**, 1400–1408.
- Smedman, A.-S.: 1991, 'Some Turbulence Characteristics in Stable Atmospheric Boundary Layer Flow', *J. Atmos. Sci.* **48**, 856–868.
- Smedman, A.-S., Högström, U., and Bergström, H.: 1997, 'The Turbulence Regime of a Very Stable Marine Airflow with Quasi-frictional Decoupling', *J. Geophys. Res.* **102**(C9), 21,049–21,059.
- Smedman, A.-S., Tjernström, M., and Högström, U.: 1993, 'Analysis of the Turbulence Structure of a Marine Low-Level Jet', *Boundary-Layer Meteorol.* **66**, 105–126.
- Smith, S. D., Anderson, R. J., den Hartog, G., Topham, D. R., and Perkin, R. G.: 1983, 'An Investigation of a Polynya in the Canadian Archipelago, 2, Structure of Turbulence and Sensible Heat Flux', *J. Geophys. Res.* **88**(C5), 2900–2910.
- Stull, R. B.: 1988, *An Introduction to Boundary Layer Meteorology*, Kluwer Academic Publishers, Dordrecht, 666 pp.
- Thorpe, A. J. and Guymer, T. H.: 1977, 'The Nocturnal Jet', *Quart. J. Roy. Meteorol. Soc.* **103**, 633–653.
- Walden, V. P., Mahesh, A., and Warren, S. G.: 1996, 'Comment on "Recent Changes in the North American Arctic Boundary Layer in Winter" by R. S. Bradley et al.', *J. Geophys. Res.* **101**(D3), 7127–7134.
- Walter, B. and Overland, J. E.: 1991, 'Aircraft Observations of the Mean and Turbulent Structure of the Atmospheric Boundary Layer during Spring in the Central Arctic', *J. Geophys. Res.* **96**(C3), 4663–4673.
- Zemba, J. and Friehe, C. A.: 1987, 'The Marine Atmospheric Boundary Layer Jet in the Coastal Ocean Dynamics Experiment', *J. Geophys. Res.* **92**(C2), 1489–1496.
- Zilitinkevich, S. and Mironov, D. V.: 1996, 'A Multi-limit Formulation for the Equilibrium Depth of a Stably Stratified Boundary Layer', *Boundary-Layer Meteorol.* **81**, 325–351.
- Zwally, H. J., Comiso, J. C., Parkinson, C. L., Campbell, W. J., Carsey, F. D., and Gloersen, P.: 1983, *Antarctic Sea Ice, 1973–1976: Satellite Passive-Microwave Observations*, NASA SP-459, National Aeronautics and Space Administration, Washington, D.C., 206 pp.